Polyethylene glycol-mediated blocking and monolayer morphology of an electrochemical aptasensor for malaria biomarker detection in human serum

Gabriela Figueroa-Miranda[a,b], Changtong Wu[a], Yuting Zhang[a], Lena Nörbel[a], Young Lo[c], Julian Alexander Tanner[c], Lothar Elling[b], Andreas Offenhäusser[a], Dirk Mayer[a*]

[a]Institute of Biological Information Processing, Bioelectronics (IBI-3), Forschungszentrum Jülich GmbH, Jülich, Germany

[b]Laboratory for Biomaterials, Institute for Biotechnology and Helmholtz-Institute for Biomedical Engineering, RWTH Aachen University, Aachen, Germany

[c]School of Biomedical Sciences, Li Ka Shing Faculty of Medicine, The University of Hong Kong, Pokfulam, Hong Kong Special Administrative Region

*corresponding author: dirk.mayer@fz-juelich.de (Dirk Mayer)

Abstract

Better approaches are critically needed for *in situ* point-of-care diagnostic biosensors that enable primary care physicians, or even individual patients, to directly analyze biological fluids without complicated sample pretreatments. Additional purification steps consume time, consume reagents, often require other equipment, and can introduce false-negative results. Biosensors have been modified with blocking molecules to reduce biofouling; however, the effectiveness relies on their chemical composition and morphology. Here, we used a polyethylene glycol film to suppress unspecific binding from human serum on an electrochemical malaria aptasensor. A detailed study of the variation of the chemical and morphological composition of the aptamer/polyethylene glycol mixed monolayer as a function of incubation time was conducted. Higher resistance to matrix biofouling was found for polyethylene glycol than for hydrophobic alkanethiol films. The best sensor performance was observed for intermediate polyethylene glycol immobilization times. With prolonged incubation, phase separation of aptamer, and polyethylene glycol molecules locally increased the aptamer density and thereby diminished the analyte binding capability. Remarkably, polyethylene glycols do not affect the aptasensor sensitivity but enhance the complex matrix tolerance, the dynamic range, and the limit of detection. Careful tuning of the blocking molecule immobilization is crucial to achieving high aptasensor performance and biofouling resistance.

Keywords: Malaria detection; Electrochemical aptasensor; Human serum; Polyethylene glycol blocking; Blocking optimization; AFM characterization.

1. Introduction

Malaria continued to have a high statistical incidence rate, with an estimated 228 million cases worldwide in 2018. Therefore, malaria is still considered a major public health challenge and a leading cause of morbidity and mortality, mainly in tropical and developing countries [1]. When detected on time, an infected person can be treated and cured. Thus, the World Health Organization (WHO) has expressed the need for developing highly sensitive, discriminatory, and affordable rapid diagnostic test (RDT). Currently implemented RDTs use antibodies as molecules for biomarker recognition. RDTs generally have been a positive development for malaria management, but RDTs using antibodies do have some drawbacks. Drawbacks include thermal instability and high production costs, which can be significant issues. Aptamers are gaining importance as potential alternatives to antibodies, since they are less prone to denaturation, possess low synthesis costs, and can be easily tagged by labels or anchor groups. A single-stranded DNA (ssDNA) aptamer receptor (2008s aptamer) was recently developed for the detection of malaria, which specifically recognizes *Plasmodium falciparum* lactate dehydrogenase (PfLDH) [2]. PfLDH is one of the main malaria biomarkers since it is present in all blood stages and is highly expressed for the metabolism of *Plasmodium* parasites [3,4].

A promising strategy to determine the parasitemia quantitatively is to link the aptamer receptors to electrochemical transducers. The resulting electrochemical ssDNA aptamer-based sensors (E-AB) complement the high affinity and specificity of the receptors with a highly sensitive and easy signal readout system, making them attractive for diagnostic applications. However, E-AB development is still in its infancy hampering clinical applications, while well-established protocols already exist for immunoassays based on colorimetric detection.

During aptasensor development, calibration and characterization measurements are commonly performed in a buffer medium or as *ex situ* measurements, due to fouling effects occurring in complex matrices like human serum or blood. The so call *ex situ* measurements are performed by incubating the biosensor in fully lysed blood or human serum without the need for dilution steps since the final measurement is conducted in a buffer medium, in this way avoiding the interference of matrix components during the detection measurement [5–9]. However, problems emerge when tests are performed *in situ*. *In situ* measurements, as their name suggests, are conduct within the complex medium (human serum or blood). Here, the interference of serum-born components may affect the selectivity and sensitivity of the sensor and thereby the reliability of quantitative signals by non-specific binding or screening real target

detection. To avoid such interference is commonly implemented a dilution of the concentrated sample [10–13]. In many cases, corresponding to the size of the target analyte, a high dilution of the complex matrix is required. Much recent research has focused on the implementation of E-AB sensors as point-of-care diagnostic tools [14–19]. The point-of-care implementation needs to be able to detect the biomarker directly in the biological fluid, a fact that requires the implementation of *in situ* detection.

A promising approach to suppress biofouling, on *in situ* measurements, is to cover the transducer with matrix repelling coatings. These blocking materials or molecular films fill spaces between the receptors without affecting their analyte binding capabilities. Numerous antifouling compounds have been proposed, such as zwitterionic molecules [20], peptides [21], alkanethiols [22,23], and polyethylene glycols [24]. They can generally be classified into hydrophobic and hydrophilic materials. Hydrophobicity can be beneficial for suppressing cell adhesion and increasing the charge transfer resistance during impedimetric sensing. 1-undecanethiol (UDT) is a commonly used hydrophobic blocking substance, which, however, shows unspecific interaction to hydrophobic domains of proteins [23,25]. 6-mercapto-1-hexanol (MCH) is less hydrophobic but is also widely employed as a blocking molecule due to its short length, which leaves aptamer/target interactions unaltered [13,23,26,27]. However, testing in biological fluids such as human serum often challenges the blocking capability of MCH [13,28]. To reduce unspecific adsorption, in many cases, the analyte sample is diluted, which increases the risk of false-negative testing results.

Among hydrophilic materials, polyethylene glycol (PEG) has been widely used in biomedical devices as antifouling coating since it possesses low interfacial energy in an aqueous medium. Consequently, proteins or cells closer to this material face thermodynamically unfavorable interactions that lead to their repulsion [29–31]. Owing to these antifouling properties, PEG has been used as a surface coating for a variety of sensor materials such as quartz, silicon dioxide, gold, silver, or graphene [32–38]. Recently, the implementation of polyethylene glycol has also gained attention as a blocking molecule for E-AB sensors [38–43]. However, a detailed study on the optimization of the composition of the ssDNA aptamer/PEG receptor layer and their morphology has not been reported so far.

We have previously developed an aptamer-based impedance electrochemical biosensor for malaria [13] using the 2008s PfLDH aptamer [2] and MCH as a blocking molecule. However, challenges for this system to perform the detection of the biomarker directly in biological fluids

were faced, and it was only possible to measure in serum that was less diluted than 50% (10% serum). In this paper, it was investigated how PEG blocking allowed the sensor to function in highly concentrated biological fluids and investigated the impact of the receptor layer composition on the sensor performance with a special emphasis on the PEG incubation time (Scheme 1).

<Scheme 1 here>

2. Experimental

2.1 Reagents

Malaria 2008s aptamer (5´-HO-$(CH_2)_6$-S-S-$(CH_2)_6$-O- CTG GGC GGT AGA ACC ATA GTG ACC CAG CCG TCT AC-3´) was synthesized by Friz Biochem GmbH (Neuried, Germany). The recombinant *Plasmodium falciparum* lactate dehydrogenase (PfLDH) and human lactate dehydrogenase B (hLDHB) were obtained from bacterial expression [2]. Monofunctional methoxy- polyethylene glycol thiol (PEG, 2kDa) was purchased from Creative PEGWorks (New York, USA). 25 mM Tris-HCl buffer (NaCl 0.1 M, Tris 25 mM, HCl 25 mM, pH 7.5) and high salt concentration phosphate-buffered saline (PBS, 10 mM sodium phosphate with 1 M NaCl and 1 mM Mg^{2+}, pH 7.5) were prepared. Tris (2-carboxyethyl) phosphine hydrochloride (TCEP), potassium ferricyanide ($K_3[Fe(CN)_6]$), potassium ferrocyanide ($K_4[Fe(CN)_6]$) trihydrate, human serum albumin (HSA), and human serum from human male AB plasma were purchased from Sigma-Aldrich Chemie GmbH (Germany). Bovine serum albumin (BSA) was obtained from Gibco (Germany). Ethanol and isopropanol were purchased from Merck (Darmstadt, Germany). All aqueous solutions were prepared using ultra-pure deionized water (18.2 MΩ cm, Milli-Q, Millipore, Merck, Darmstadt, Germany).

2.2 Gold rod electrode cleaning

Gold rod electrodes (2 mm in diameter) were intensively cleaned before aptamer modification; a detailed description can be found elsewhere [27]. Briefly, the gold electrodes were consecutively polished with aqueous slurries of alumina powder of 0.30 and 0.05 µm on a micro cloth. Afterward, the electrodes were sonicated in ethanol, isopropanol, and Milli-Q water for 5 min each and dried in a nitrogen stream. Finally, they were activated with electrochemical

cleaning by performing cyclic voltammetry (CV) with Autolab potentiostat/galvanostat PGSTAT302 (Eco Chemie, Netherlands) in a solution of 0.5 M NaOH with a scan range from −1.35 V to −0.35 V, 500 scans at a scan rate of 2 V/s and consecutively 0.5 M H_2SO_4 with a scan range from −0.35 V to 1.5 V, 150 scans at a scan rate of 1 V/s. The electrode area was determined by a CV in 50 mM H_2SO_4 solution with a scan range from −0.35 V to 1.5 V at a scan rate of 0.1 V/s [44].

*2.3 Stepwise preparation of the aptamer/*PEG *receptor layer*

The 2008s aptamer concentration was determined by measuring the absorbance at 260 nm with the UV/Vis/NIR spectrometer Lambda 900 (Perkin Elmer, USA). A concentration of 0.5 µM aptamer was used in all the experiments for the immobilization, otherwise specified. The aptamer was always treated with 10 mM TCEP for 1 h at room temperature to reduce the disulfide-protecting bond before incubation, enabling the direct binding of the thiol group of the aptamer to the gold surface. After the pre-treatment, the 2008s aptamer was diluted in 10 mM high salt concentration PBS buffer to a final volume of 250 µL. Then, the cleaned gold electrode was incubated by immersing it in the aptamer solution overnight. Afterward, the aptamer-modified electrode was rinsed with Tris buffer and consecutively with Milli-Q water to remove excess aptamer molecules. Subsequently, the gold electrode was incubated with an aqueous solution containing 5 mg/mL PEG for the indicated time. Last, a rinsing step with Tris buffer was performed to remove non-covalently bound blocking molecules. Once the aptasensor was ready, the different PfLDH protein concentrations were detected. In the same way, the control proteins (BSA, HSA, and hLDH) used for the selectivity test were investigated with a concentration of 50 nM prepared similarly to the PfLDH protein sample.

2.4 In situ and ex situ PfLDH detection

The impedance measurements were recorded at 45 min after addition of the respective concentration of PfLDH (7.14 µM stock solution) in 1 mL volume of 1:1 ratio human serum to 25 mM Tris-HCl buffer solution at 7.5 pH containing 5 mM $[Fe(CN)_6]^{3-/4-}$ for *in situ* measurements. For *ex situ* measurements, the sensor was incubated for 45 min in whole human serum with the correspondingly added PfLDH concentration, posteriorly rinse with buffer, and

measured in 5 mM $[Fe(CN)_6]^{3-/4-}$ in 25 mM Tris-HCl buffer solution. In either case, the external standard addition method was used.

2.5 Electrochemical impedance spectroscopy measurements

Electrochemical impedance spectroscopy (EIS) measurements were performed with an Autolab potentiostat/galvanostat PGSTAT302 (Eco Chemie, Netherlands) consisting of a three-electrode system. Therefore, a platinum wire was utilized as the counter electrode (CE), an Ag/AgCl electrode (DriRef2, WPI Germany) as the reference electrode (RE), and the gold rod electrode with the immobilized aptamer/PEG mixed monolayer as the working electrode (WE). All potentials in this work are noted with respect to a saturated Ag/AgCl reference electrode. A potential bias of 0.22 V was applied to the electrode superimposed by an alternating voltage in a frequency range from 10 kHz to 1 Hz with an amplitude of 0.01 V. The NOVA 2.1 software was used for fitting EIS data according to the electrical equivalent circuit in order to obtain the fit-component parameter values.

2.6 QCM-D measurements

The Quartz Crystal Microbalance with Dissipation monitoring (QCM-D) equipped with a fluidic system from Q-sense Biolin Scientific (Västra Frölunda, Schweden) was used to analyze the mass change and the associated viscoelastic properties of the system after each immobilization step [45]. Firstly, the QCM-D components and gold sensors were cleaned according to recommendations from the supplier. The QCM gold chips were cleaned in an oxygen plasma oven for 3 min at 50% power and 0.5 mbar. Later, they were left in ethanol for 30 min to reduce back the gold oxide formed. Once everything was cleaned, the cell was mounted, and the sensor was placed on the module. The buffer solution was pumped through the cell and left running until stabilization of the sensor signal was achieved (frequency shift below 0.2 Hz in 10 min). Subsequently, the experiment was started by consecutively flushing molecule solutions and posterior rinsing Tris buffer through the QCM-D fluidic cell.

2.7 XPS analysis

The chemical sample analysis for corroboration of aptamer and PEG immobilization by X-ray photoelectron spectroscopy (XPS) was conducted with the instrument Phi5000 Versa Probe II (ULVAC-Phi Inc., USA). The source used was the monochromatic Al K-alpha line (hν = 1.486 keV), with the following power: 50 W at 15 kV, 200 μm spot size, 187.5 eV pass energy, 0.8 eV step, 100 ms/step.

2.8 AFM analysis

Atomic force microscopy (AFM) imaging was performed using a Nanoscope Multimode 8 microscope (Bruker, Netherlands) equipped with a piezoelectric E-series scanner and aluminum-coated Si cantilever from Bruker (RTESPA-150) with a resonant frequency of 150 kHz and spring constant 5 N/m. The images were acquired in tapping mode with the following parameters: scan rate 1 Hz, scan size 0.5 μm, and aspect ratio 1:1. The (111) plane of a gold single crystal disk was used as a model electrode surface. The activation and cleaning of the single crystal were done by thoroughly rinsing it in ethanol, isopropanol, and Milli-Q water. After drying, the crystal was annealed for 10 min in a hydrogen flame (orange glowing) and cooled down to room temperature in an argon stream. The subsequent aptamer modification and PEG blocking were done, as described in section 2.3.

3. Results and discussion

The detection of biomarkers by E-AB aptasensors in biological fluids like human serum or blood remains a challenge due to undesired non-specific adsorption of matrix species on the surface of the transducer [28,46,47]. Here we present the detection of PfLDH in human serum by the implementation and optimization of a polyethylene glycol (PEG) monolayer as a blocking coating.

3.1 Reduction of non-specific adsorption

In our previous report, noticeable non-specific binding of PfLDH was observed in human serum on a receptor-free gold surface covered only with MCH blocking molecules, which caused an appreciated semicircular impedance increment of 33.9±2.4 % in the Nyquist plot representation,

(Fig. 1a) [13]. The Nyquist plot displays the real versus the imaginary part of the impedance, showing the characteristic formation of a semicircle at higher frequencies (charge transfer control processes) and a straight line at low frequencies (diffusion control processes). The electrical equivalent circuit elements used to fit the impedance measurements are shown in equivalent Randles circuit at the limit of high-frequency [48], inset Fig.1a. The equivalent circuit model used here comprises a resistor for the intrinsic electrolyte resistance (R_s) in series with a parallel constant phase element (CPE), and a charge transfer resistance (R_{ct}). The R_{ct} is the main element used here to calculate the percentage change of the charge transfer resistance by PfLDH detection [13].

A distinctly smaller non-specific binding corresponding to only 8.8±1.2 % impedance change was observed in this study for a PEG-modified receptor-free sensor surface after exposure to 50 nM PfLDH in human serum (Fig. 1b). The mechanism behind the protein repulsion by PEG has been reported to be a consequence of the low gain of adhesion enthalpy and the associated loss of entropy due to steric repulsion during the interaction process. That means that the steric repulsion is related to restrictions of configurational freedom and concomitant desolvation of PEG when the protein tries to attach to the surface, making it a thermodynamically unfavorable interaction [29,30,49,50]. Noteworthy, also recent publications have demonstrated PEG antifouling capabilities for aptamer/PEGylated surfaces in complex matrices like serum or blood [40,42,43]. However, systematic studies on the correlation of ssDNA aptamer/PEG-film composition and antifouling properties for enhanced target detection, to the best of our knowledge, have not been reported so far. Zhang *et al.* reported that an increase in the concentration of a zwitterion-bifunctionalized poly (ethylene glycol) decreases the signal of the ATP analyte [43]. What remains unknown so far is how the signal changes for low and high PEG surface density, how the morphology of the mixed aptamer/PEG monolayer alters for different incubation times of thiolated PEG molecules, and how these changes influence the sensor performance.

<Fig. 1 here>

3.2 Physicochemical characterization methods for stepwise aptasensor fabrication with different PEG *blocking times*

3.2.1 Monitoring stepwise molecule adsorption by QCM

Firstly, the stepwise immobilization of aptamer, PEG, and PfLDH detection was monitored by Quartz Crystal Microbalance with Dissipation (QCM-D). This method facilitated the determination of changes in mass and the viscoelastic properties of the mixed receptor layer during its assembling. The QCM-D sensor oscillates to its resonance frequency driven by an alternating voltage applied to the sensor. The frequency decreases, and the dissipation changes when a molecular film binds to the sensor surface due to the added mass of the molecules and the energy dissipation associated with the molecule's softness, respectively [51]. For thin and rigid films, the frequency change is proportional to the mass increase, which can be calculated with the Sauerbrey equation [45]:

$$\Delta f = \frac{2 f_0^2}{A \sqrt{\rho_q \mu_q}} \Delta m \quad (1)$$

f_0^2 stands for the resonant frequency of the fundamental mode (Hz), Δf is the frequency change, Δm is the mass change, A is the area of the piezoelectrically active crystal, ρ_q is the density of quartz (ρ_q= 2.648 g/cm^3), and μ_q is the shear modulus of the quartz for AT-cut crystal (μ_q = 2.947×10^{11} g/cm s^2).

The application of 0.5 µM aptamer to a bare Au sensor and subsequent Tris rinsing caused a decrement in the frequency (Δf = 21.1 Hz) associated with the immobilization of the aptamer receptor, Fig. 2a, and b. The corresponding calculated mass was 2.50 ng/mm^2 corroborating the aptamer film formation [52]. The increase in the dissipation (ΔD = 1.55 ppm) is correlated with the soft and elastic nature of ssDNA aptamers and corroborated by elastic modulus (E) and viscosity (μ) reported in the literature, Table S1 [53,54]. After the addition of PEG blocking molecules (7 h incubation) and rinsing with Tris buffer, a further frequency shift of 2.9 Hz was observed due to the binding of these molecules to the aptamer-free electrode spaces (Fig 2c). The associated mass change was 0.16 ng/mm^2. The relatively small change of the frequency after PEG addition in comparison to aptamer incubation indicates that aptamer receptors already occupied the majority of the sensor surface. The dissipation increase (0.34 ppm) is correlated to the soft and hydrated nature of the PEG in agreement with previously reported values for elastic modulus and viscosity [55,56]. According to the QCM-D experiments, there was no significant frequency and dissipation change for different PEG incubation times, suggesting that the PEG density did not change noticeably during extended incubation (Fig. S1). Also, E and μ for 2 and 16 h did not indicate any significant change for different PEG incubation times,

Table S1. Only for 16 h PEG incubation, a minor thickness increment was observed. Further frequency changes of Δf = 0.7 Hz (0.12 ng/mm^2) and 4.8 Hz (0.84 ng/mm^2) were registered after the addition of 10 nM and 50 nM of PfLDH, respectively, as well as a slight dissipation change of ΔD = 0.07 and 0.41 ppm, which are assigned to the protein binding via aptamer receptors, Fig. 2d. The small mass change associated with the protein detection might be related to the fact that the proteins are not directly bound to the electrode surface but via the aptamer, which limits the detection capabilities of this method [51].

<Fig. 2 here>

3.2.2 XPS investigations

The chemical composition of the bare gold electrode, the electrode after modification with aptamer, and the complete aptamer/PEG receptor layer were investigated by x-ray photoelectron spectroscopy (XPS). Fig. 3 shows the survey spectra of the different samples, which are mainly dominated by the peaks of the Au substrate. Compared with the bare gold (blue spectrum), a decrement of the gold signal (Au 4f) was observed after aptamer and PEG adsorption due to the formation of a mixed SAM on top of Au. An increment of the carbon (C 1s) content, the appearance of oxygen (O 1s), nitrogen (N 1s), and phosphorus (P 2p) peaks confirmed the aptamer immobilization since those are the main elements of ssDNA (red spectrum). Further increments of carbon and oxygen were observed together with a decrease of Au 4f, and N 1s after the long-chain PEG (2 kDa) was immobilized. The sulfur (S 2p) peak was caused by the thiol-terminal group that anchors aptamer and PEG to the gold surface [50,57]. The height of this peak was relatively small since each molecule possesses one sulfur atom, which was buried by the entire chain of the molecule. The extension of the PEG immobilization time did not lead to an apparent change of the C1s or O1s signals similar to QCM-D data indicating that the coverage increase was beyond the accuracy of used measurement methods, Table. S2.

Contact angle experiments corroborated the immobilization of aptamer and PEG molecules via decreasing contact angles from 84.2° for the bare gold to 27.6° for only PEG and approximately 16.0° for aptamer alone as well as aptamer/PEG mixed monolayers. These contact angle variations indicate enhanced hydrophilicity for the surface after aptamer, PEG, and

aptamer/PEG layer formation (Fig. S2). An analysis of the contact angle was also done for different PEG immobilization times. The contact angle remained similar or slightly smaller than those of the PEG-free aptamer electrode and distinctly smaller than those of PEG/AuE, which confirms the dominating influence of the aptamer on the composition and surface energy of the mixed aptamer/PEG receptor layer (Table S3).

<Fig. 3 here>

3.2.3 AFM investigations

The topographical characterization of the surface morphology after aptamer immobilization and different PEG incubation times was performed by AFM analysis. The preparation started from an atomically flat gold (111) single crystal surface, which had an RMS surface roughness of 0.07±0.01 nm, Fig 4a, and b. After aptamer immobilization, the overall surface roughness increased to 0.20±0.02 nm. Spherical objects were homogeneously distributed over the surface and possessed a topographical height of 0.83±0.10 nm, Fig 4c, and d. It can be assumed that the aptamer molecules adsorbed to the surface in islands and did not form a dense monolayer. This assumption is based on the one hand on our AFM data since a dense monolayer would result in smaller surface roughness [58]. On the other hand, the aptamer surface density was calculated by chronocoulometry, which was $(1.29\pm0.01)\times10^{12}$ molecules/cm^2 and corresponded to a low-density coverage, according to Zhang *et al.* [59]. After the incubation of PEG for 2h, the roughness further increased to 0.32±0.03nm with feature heights of 1.07±0.16 nm, suggesting that also these molecules bind to the gold surface (Fig. 4e and f). However, aptamer and blocking molecules did not form a homogeneously mixed monolayer but seemingly separated into domains, which appeared as elevated islands in the AFM images.

Systematic analysis of the surface roughness, island height, and island diameter for two different aptamer concentrations showed in both cases for different PEG incubation times an increase in all, roughness, island height, and island diameter, Table S4. Noteworthy, the increase in these parameters was more significant for high aptamer densities. In particular, the number of high islands was less for 2 h PEG incubation as compared with 7 h for both aptamer densities. That, together with the increase in surface roughness, indicated that the aptamer molecules tethered to the electrode surface initially not only via thiol-gold bonds but also via

weak nitrogen-gold interactions [57,60]. After the addition of PEG, these molecules bound to free gold areas and pushed aptamer molecules upright that were previously lying on the surface. This event was seemingly not so significant for short PEG immobilization times (2 h) (Fig. 4e) but increased after 7 h and 16 h PEG incubation, which lifts ssDNA aptamers and increased the number of high islands (Fig 4g). Although the PEG surface coverage did not change significantly for 7 and 16 h, as corroborated by QCM-D and XPS measurements, there was a distinct surface rearrangement between aptamer and PEG for different incubation times. For 16 h incubation, a distinct increase in the island diameter was observed, indicating that a ripening process occurred where the aptamer islands merged to connected domains resulting in phase-separated arrangements (Fig. 4i). The island formation indicates that short ssDNA and PEG molecules were subjected to phase separation and instead behaved like ssDNA/alkanethiol SAM [61–63]. The different alkyl chain length connected to the respective thiol group of ssDNA and PEG might contribute to this observation.

<Fig. 4 here>

3.3 PEG blocking time optimization

The composition of the mixed receptor layer is crucial for sensor performance. On the one hand, the aptamer receptor (here 2008s) requires a particular space on the transducer surface for 3-D conformational adaptation when binding with its target (PfLDH). On the other hand, those electrode surface areas that are not covered by aptamers should be blocked by PEG to reduce the non-specific binding of components present in human serum. Therefore, impedance measurements for the detection of PfLDH at different incubation times of PEG were performed to identify the optimal blocking conditions (Fig 5). At short PEG incubation time (< 5 h), the target detection signal, which represents the change of the charge transfer resistance induced by target binding divided by initial charge transfer resistance, $\Delta R_{ct}/R_{ct0}$, was low due to the low density of the blocking molecules. The ssDNA molecules partially interacted with the Au electrode surface, which competed with the analyte binding, corroborated by AFM analysis (Fig 4e). With increasing incubation times, the detection signal rose, since ssDNA/Au interactions were cleaved by PEG binding until the PfLDH signal reached its maximum at 7 hours. Besides, a shorter PEG molecule (400 Da) was also tested at 7 h incubation time for

PfLDH detection in human serum. A lower antifouling capability was observed as compared to the longer PEG (2 kDa) blocking molecule (Fig. S3).

Interestingly, as the incubation time increased (> 9 h), a highly compact PEG monolayer was obtained, which led to a decrement of the signal by inhibiting the interaction between the aptamer and its target, also corroborated by AFM analysis (Fig 4i). Both high aptamer and PEG densities may contribute to his observation. As mentioned before, aptamer requires conformational freedom to adapt to its target. If their densities are too high, the analyte binding capability vanishes. Furthermore, it has been reported that densely packed PEGylated surfaces with brush-like configuration do not effectively prevent protein adsorption. Only, less packed crystalline helical amorphous forms, mushroom configuration, are resistant to adsorption of proteins. The different configurations are correlated with the incubation time. Densely packed assemblies were reported for times exceeding overnight incubation, while short incubation times (≤2 h) were not enough to immobilize PEG for effectively avoiding protein adsorption [30,50,64]. The phase separation observed in the AFM study (Fig. 4i) was companied by an increase of molecule packing within its respective domain. These effects could explain the signal reduction for the impedance measurements since the phase separation, which enhances the island formation, increases the local aptamer density making them not accessible for the interaction with the target PfLDH.

<Fig. 5 here>

3.4 Concentration dependence of sensor signal

The sensitivity is doubtless, an important parameter for biosensors, which should cover the entire pathologically relevant concentration range, including healthy and disease-related biomarker levels. A calibration curve was recorded to determining the lowest confidence detection value by calculating the limit of detection (LOD), the dynamic range of detection, and sensor sensitivity. The obtained equation from the logarithmic presentation of the PfLDH concentration versus relative charge transfer resistance change for the aptamer/MCH modified sensor was $\Delta R_{ct}/R_{ct0}$ (%) = 8.3 lg$C$ + 16.0 with a correlation coefficient of 0.99. The following equation was used to calculate the limit of detection: LOD = ks/m, where k is the constant of random error (3 is the typical value used as the signal-to-noise ratio), s the standard deviation

of the blank, and *m* the slope of the calibration curve [13]. Such aptamer/MCH modified sensor showed a LOD of 1.3±0.1 pM and a dynamic detection range from 10.0 pM to 10.0 nM in 10% HS (Fig 6a). It is worthy of mentioning that it was only possible to detect the target protein in human serum after dilution to 10 %. In serum concentration of 50 % or higher, no detectable signal change was observed (data not included). The sensitivity (S) of the sensor can be extracted from the slope of the semi-logarithmic equation being S = 8.3±0.1 /nM. The obtained equation for the aptamer/PEG receptor layer was $\Delta R_{ct}/R_{ct0}$ (%) = 7.9 lg$C$ + 33.9 with a correlation coefficient of 1.00. This aptamer/PEG sensor exhibited a lower LOD of 0.8 pM and a wider dynamic concentration range that goes from 2.3 pM to 100.0 nM in significantly higher serum concentration (50% HS), Fig 6b. The Nyquist plot with the different PfLDH concentrations tested is shown in Fig S4a. Interestingly, the sensor sensitivity was not considerably affected (S = 7.9±0.1 /nM), indicating that the analyte binding capability of the receptor remains unaltered by choice of the blocking molecule. The implementation of PEG as blocking molecule significative enhanced the tolerance for the detection of spiked PfLDH in highly concentrated human serum. Plus, it allowed de detection of PfLDH in a wide range of concentrations, covering the clinical relevant range of detection. The reported clinical concentration of PfLDH is found between few pM to hundreds of nM, which correlates with the percentage of the parasitemia infection [3,65,66].

<Fig. 6 here>

The *ex situ* detection for the PEG containing sensor was also tested, and the obtained equation, in this case, was $\Delta R_{ct}/R_{ct0}$ (%) = 7.2 lg$C$ + 51.1 with a correlation coefficient of 0.98. The calculated LOD was similar to the Aptamer/MCH sensor (1.5 pM), although the aptasensor was incubated in whole human serum, and subsequently measured in Tris buffer. The dynamic detection range (4.5 pM to 100.0 nM) and the sensitivity (S = 7.2 /nM) were similar to *in situ* experiments, Fig 6c. That also indicates that the sensor´s sensitivity is mainly independent of the implementation of the measurement (*in situ* or *ex situ*), but rather, the blocking molecule enhances the matrix tolerance, the LOD, and the detectable dynamic detection range.

Table 1 summarizes the aptasensor parameters of PfLDH detection, including literature and the present work for *in situ* and *ex situ* detection. Compared with previously reported characteristics, the new aptasensor presented here with PEG as a blocking molecule possessed the lowest LOD and the most extensive dynamic range of detection for *in situ* measurements. Also, this new aptasensor allowed PfLDH detection in less diluted (50%) human serum while

previous works, including our own, using MCH as blocking molecule facilitated the detection only in high diluted serum (10%). In the case of *ex situ* measurements, our easy to operate electrochemical aptasensor exhibited similar performance to state-of-the-art optical biosensors in whole human serum.

<Table 1 here>

3.5 Sensor selectivity

The blocking film has an impact also on the selectivity, which is an important parameter not only for clinical but also for point-of-care detection since elaborated pretreatments cannot be applied for that application. Therefore, the aptasensor response was also challenged versus other serum components such as human serum albumin (HSA) and human lactate dehydrogenase B (hLDHB). HSA is the most abundant protein in human blood plasma, while hLDHB is the human analog of the analyte with many structural correlations to PfLDH. Both can considerably interfere with the detection of PfLDH. For these experiments, the control proteins were spiked independently in the corresponding 50% human serum sample. Our malaria aptasensor exhibited a more significant impedance change for PfLDH compared to those compounds. Bovine serum albumin (BSA), HSA, and hLDHB caused only a marginally impedance change, although they were added at comparable high concentrations of PfLDH (Fig 7). In Figure S4b, the Nyquist plot is shown with the marginal unspecific detection of the control protein BSA. The selectivity versus human LDH was established already during the SELEX process by a counter target selection of the aptamer, indicating that the PEG blocking does not impair the selectivity of the aptamer receptor [2]. Furthermore, the long-term repulsion of serum protein was evaluated by impedance measurements at different incubation times in human serum. Only nonsystematic variations of the charge transfer resistance over time were observed, demonstrating the short-term stability of the PEG-modified aptasensor (Fig. S5a). However, at the long-term storage of the aptasensor, a considerable degradation of the signal was detected (Fig S5b). This observation might be associated with continuous phase separation of the PEG and aptamer molecules since a single thiol anchoring group might not be enough to prevent molecule segregation effectively in the long term. The possible implementation of aptamer molecules with multiple anchoring thiol groups might help to avoid this phenomenon [69].

<Fig. 7 here>

4. Conclusion

In this work, we report on the reduction of non-specific adsorption and enhancement of PfLDH detection, based on impedance measurements, in a complex matrix such as human serum by optimizing the incubation of PEG blocking molecules. Impedance investigations, together with AFM characterization, XPS, and QCM-D analysis, suggested that the overall density of PEG did not distinctly change for different incubation times, but the morphology of the mixed receptor layer did. In fact, the incubation time significantly influences the aptamer/PEG system by cleaving weak bonds between ssDNA chains and Au, lifting the aptamer molecules driven by the covalent adsorption of PEG molecules. This liberation of the receptor strands enhanced the target binding capability of the sensor for short incubation times. However, after 9 hours of incubation and longer, declining sensor signals were observed, which can be assigned to a phase separation between aptamer and PEG molecules. AFM investigations suggest that the phase separation locally increased the aptamer density and thereby degrades their binding capability to PfLDH due to a restricted conformational degree of freedom. Comparing the calibration curves of aptasensors using hydrophobic MCH or hydrophilic PEG revealed that the blocking molecule had no impact on the sensor sensitivity but strongly enhances the matrix tolerance, the dynamic range, and the limit of detection. Our PEG/aptamer receptor system worked reliably in 50% diluted and full serum for *in situ* and *ex situ* detection, respectively, and reached its optimal working conditions after 7 h PEG incubation time. That represents a remarkable improvement towards the desired *in situ* detection for point-of-care testing. Further work is conducted in our laboratory to implement multi-thiol anchoring groups that might prevent phase separation at long incubation times and enhance the target detection in full blood or human serum samples.

Acknowledgements

This research work was supported by the Mexican National Council for Science and Technology and the German Academic Exchange Service (grant number: 448904).

Author contributions

Gabriela Figueroa-Miranda: designed and conducted experiments, data analysis, writing – original draft and editing. Changtong Wu: contributed experimental work, writing – review and editing. Yuting Zhang: contributed experimental work, writing – review. Lena Nörbel: contributed experimental work, data analysis. Young Lo: contributed reagents/materials tools, writing – review. Julian Alexander Tanner: contributed reagents/materials tools, writing – review and editing. Lothar Elling: contributed writing – review and editing. Andreas Offenhäusser: contributed writing – review and editing. Dirk Mayer: conducted experiments, data analysis, and writing – original draft and editing.

References

[1] World malaria report 2019, (n.d.). https://www.who.int/publications-detail/world-malaria-report-2019 (accessed December 22, 2019).

[2] Y.-W. Cheung, J. Kwok, A.W.L. Law, R.M. Watt, M. Kotaka, J.A. Tanner, Structural basis for discriminatory recognition of Plasmodium lactate dehydrogenase by a DNA aptamer, Proc. Natl. Acad. Sci. 110 (2013) 15967–15972. https://doi.org/10.1073/pnas.1309538110.

[3] J.W. Jang, C.H. Cho, E.T. Han, S.S.A. An, C.S. Lim, pLDH level of clinically isolated Plasmodium vivax and detection limit of pLDH based malaria rapid diagnostic test, Malar. J. 12 (2013) 181. https://doi.org/10.1186/1475-2875-12-181.

[4] R. Piper, J. Lebras, L. Wentworth, A. Hunt-Cooke, S. Houzé, P. Chiodini, M. Makler, Immunocapture diagnostic assays for malaria using Plasmodium lactate dehydrogenase (pLDH)., Am. J. Trop. Med. Hyg. 60 (1999) 109–118.

[5] T. Bryan, X. Luo, P.R. Bueno, J.J. Davis, An optimised electrochemical biosensor for the label-free detection of C-reactive protein in blood, Biosens. Bioelectron. 39 (2013) 94–98. https://doi.org/10.1016/j.bios.2012.06.051.

[6] R.M. Dirkzwager, S. Liang, J.A. Tanner, Development of Aptamer-Based Point-of-Care Diagnostic Devices for Malaria Using Three-Dimensional Printing Rapid Prototyping, ACS Sens. 1 (2016) 420–426. https://doi.org/10.1021/acssensors.5b00175.

[7] N.K. Singh, P. Jain, S. Das, P. Goswami, Dye Coupled Aptamer-Captured Enzyme Catalyzed Reaction for Detection of Pan Malaria and P. falciparum Species in Laboratory Settings and Instrument-Free Paper-Based Platform, Anal. Chem. 91 (2019) 4213–4221. https://doi.org/10.1021/acs.analchem.9b00670.

[8] M. Xu, X. Luo, J.J. Davis, The label free picomolar detection of insulin in blood serum, Biosens. Bioelectron. 39 (2013) 21–25. https://doi.org/10.1016/j.bios.2012.06.014.

[9] N.K. Singh, S.K. Arya, P. Estrela, P. Goswami, Capacitive malaria aptasensor using Plasmodium falciparum glutamate dehydrogenase as target antigen in undiluted human serum, Biosens. Bioelectron. 117 (2018) 246–252. https://doi.org/10.1016/j.bios.2018.06.022.

[10] N.K. Singh, P.D. Thungon, P. Estrela, P. Goswami, Development of an aptamer-based field effect transistor biosensor for quantitative detection of Plasmodium falciparum glutamate dehydrogenase in serum samples, Biosens. Bioelectron. 123 (2019) 30–35. https://doi.org/10.1016/j.bios.2018.09.085.

[11] B. Chakma, P. Jain, N.K. Singh, P. Goswami, Development of Electrochemical Impedance Spectroscopy Based Malaria Aptasensor Using HRP-II as Target Biomarker, Electroanalysis. 30 (2018) 1847–1854. https://doi.org/10.1002/elan.201800142.

[12] N.K. Singh, B. Chakma, P. Jain, P. Goswami, Protein-Induced Fluorescence Enhancement Based Detection of Plasmodium falciparum Glutamate Dehydrogenase Using Carbon Dot Coupled Specific Aptamer, ACS Comb. Sci. 20 (2018) 350–357. https://doi.org/10.1021/acscombsci.8b00021.

[13] G. Figueroa-Miranda, L. Feng, S.C.-C. Shiu, R.M. Dirkzwager, Y.-W. Cheung, J.A. Tanner, M.J. Schöning, A. Offenhäusser, D. Mayer, Aptamer-based electrochemical biosensor for highly sensitive and selective malaria detection with adjustable dynamic response range and reusability, Sens. Actuators B Chem. 255 (2018) 235–243. https://doi.org/10.1016/j.snb.2017.07.117.

[14] N. Arroyo-Currás, J. Somerson, P.A. Vieira, K.L. Ploense, T.E. Kippin, K.W. Plaxco, Real-time measurement of small molecules directly in awake, ambulatory animals, Proc. Natl. Acad. Sci. 114 (2017) 645–650. https://doi.org/10.1073/pnas.1613458114.

[15] B.S. Ferguson, D.A. Hoggarth, D. Maliniak, K. Ploense, R.J. White, N. Woodward, K. Hsieh, A.J. Bonham, M. Eisenstein, T.E. Kippin, K.W. Plaxco, H.T. Soh, Real-Time, Aptamer-Based Tracking of Circulating Therapeutic Agents in Living Animals, Sci. Transl. Med. 5 (2013) 213ra165-213ra165. https://doi.org/10.1126/scitranslmed.3007095.
[16] Z. Hao, Z. Wang, Y. Li, Y. Zhu, X. Wang, C.G.D. Moraes, Y. Pan, X. Zhao, Q. Lin, Measurement of cytokine biomarkers using an aptamer-based affinity graphene nanosensor on a flexible substrate toward wearable applications, Nanoscale. 10 (2018) 21681–21688. https://doi.org/10.1039/C8NR04315A.
[17] J. Tu, R.M. Torrente-Rodríguez, M. Wang, W. Gao, The Era of Digital Health: A Review of Portable and Wearable Affinity Biosensors, Adv. Funct. Mater. (2019). https://doi.org/10.1002/adfm.201906713.
[18] L. Bezinge, A. Suea-Ngam, A. J. deMello, C.-J. Shih, Nanomaterials for molecular signal amplification in electrochemical nucleic acid biosensing: recent advances and future prospects for point-of-care diagnostics, Mol. Syst. Des. Eng. (2020). https://doi.org/10.1039/C9ME00135B.
[19] S. Liang, A.B. Kinghorn, M. Voliotis, J.K. Prague, J.D. Veldhuis, K. Tsaneva-Atanasova, C.A. McArdle, R.H.W. Li, A.E.G. Cass, W.S. Dhillo, J.A. Tanner, Measuring luteinising hormone pulsatility with a robotic aptamer-enabled electrochemical reader, Nat. Commun. 10 (2019) 1–10. https://doi.org/10.1038/s41467-019-08799-6.
[20] Y. Hu, B. Liang, L. Fang, G. Ma, G. Yang, Q. Zhu, S. Chen, X. Ye, Antifouling Zwitterionic Coating via Electrochemically Mediated Atom Transfer Radical Polymerization on Enzyme-Based Glucose Sensors for Long-Time Stability in 37 °C Serum, Langmuir. 32 (2016) 11763–11770. https://doi.org/10.1021/acs.langmuir.6b03016.
[21] T. Date, T. Sawada, T. Serizawa, Self-assembled peptides on polymer surfaces: towards morphology-dependent surface functionalization, Soft Matter. 9 (2013) 3469–3472. https://doi.org/10.1039/C3SM27841G.
[22] C.-Y. Lee, P. Gong, G.M. Harbers, D.W. Grainger, D.G. Castner, L.J. Gamble, Surface Coverage and Structure of Mixed DNA/Alkylthiol Monolayers on Gold: Characterization by XPS, NEXAFS, and Fluorescence Intensity Measurements, Anal. Chem. 78 (2006) 3316–3325. https://doi.org/10.1021/ac052137j.
[23] L. Feng, A. Sivanesan, Z. Lyu, A. Offenhäusser, D. Mayer, Electrochemical current rectification–a novel signal amplification strategy for highly sensitive and selective aptamer-based biosensor, Biosens. Bioelectron. 66 (2015) 62–68. https://doi.org/10.1016/j.bios.2014.10.057.
[24] S. Sharma, R.W. Johnson, T.A. Desai, XPS and AFM analysis of antifouling PEG interfaces for microfabricated silicon biosensors, Biosens. Bioelectron. 20 (2004) 227–239. https://doi.org/10.1016/j.bios.2004.01.034.
[25] L. Feng, Z. Lyu, A. Offenhäusser, D. Mayer, Electrochemically triggered aptamer immobilization via click reaction for vascular endothelial growth factor detection, Eng. Life Sci. 16 (2016) 550–559. https://doi.org/10.1002/elsc.201600068.
[26] Y. Xiao, R.Y. Lai, K.W. Plaxco, Preparation of electrode-immobilized, redox-modified oligonucleotides for electrochemical DNA and aptamer-based sensing, Nat. Protoc. 2 (2007) 2875–2880. https://doi.org/10.1038/nprot.2007.413.
[27] Y. Zhang, G. Figueroa-Miranda, Z. Lyu, C. Zafiu, D. Willbold, A. Offenhäusser, D. Mayer, Monitoring amyloid-β proteins aggregation based on label-free aptasensor, Sens. Actuators B Chem. 288 (2019) 535–542. https://doi.org/10.1016/j.snb.2019.03.049.
[28] S. Lee, K.-M. Song, W. Jeon, H. Jo, Y.-B. Shim, C. Ban, A highly sensitive aptasensor towards Plasmodium lactate dehydrogenase for the diagnosis of malaria, Biosens. Bioelectron. 35 (2012) 291–296. https://doi.org/10.1016/j.bios.2012.03.003.

[29] A. Anne, C. Demaille, J. Moiroux, Terminal Attachment of Polyethylene Glycol (PEG) Chains to a Gold Electrode Surface. Cyclic Voltammetry Applied to the Quantitative Characterization of the Flexibility of the Attached PEG Chains and of Their Penetration by Mobile PEG Chains, Macromolecules. 35 (2002) 5578–5586. https://doi.org/10.1021/ma020071d.
[30] P. Harder, M. Grunze, R. Dahint, G.M. Whitesides, P.E. Laibinis, Molecular Conformation in Oligo(ethylene glycol)-Terminated Self-Assembled Monolayers on Gold and Silver Surfaces Determines Their Ability To Resist Protein Adsorption, J. Phys. Chem. B. 102 (1998) 426–436. https://doi.org/10.1021/jp972635z.
[31] N. Liu, Z. Xu, A. Morrin, X. Luo, Low fouling strategies for electrochemical biosensors targeting disease biomarkers, Anal. Methods. 11 (2019) 702–711. https://doi.org/10.1039/C8AY02674B.
[32] N.M. Andoy, M.S. Filipiak, D. Vetter, Ó. Gutiérrez-Sanz, A. Tarasov, Graphene Biosensors: Graphene-Based Electronic Immunosensor with Femtomolar Detection Limit in Whole Serum (Adv. Mater. Technol. 12/2018), Adv. Mater. Technol. 3 (2018) 1870046. https://doi.org/10.1002/admt.201870046.
[33] K. Emoto, J.M. Harris, J.M. Van Alstine, Grafting Poly(ethylene glycol) Epoxide to Amino-Derivatized Quartz: Effect of Temperature and pH on Grafting Density, Anal. Chem. 68 (1996) 3751–3757. https://doi.org/10.1021/ac960114m.
[34] P. Li, K. Greben, R. Wördenweber, U. Simon, A. Offenhäusser, D. Mayer, Tuning neuron adhesion and neurite guiding using functionalized AuNPs and backfill chemistry, RSC Adv. 5 (2015) 39252–39262. https://doi.org/10.1039/C5RA06901G.
[35] X. Luo, Q. Xu, T. James, J.J. Davis, Redox and Label-Free Array Detection of Protein Markers in Human Serum, Anal. Chem. 86 (2014) 5553–5558. https://doi.org/10.1021/ac5010037.
[36] A. Q. Tran, C. Kaulen, U. Simon, A. Offenhäusser, D. Mayer, Surface coupling strength of gold nanoparticles affects cytotoxicity towards neurons, Biomater. Sci. 5 (2017) 1051–1060. https://doi.org/10.1039/C7BM00054E.
[37] S. Schilp, A. Rosenhahn, M.E. Pettitt, J. Bowen, M.E. Callow, J.A. Callow, M. Grunze, Physicochemical Properties of (Ethylene Glycol)-Containing Self-Assembled Monolayers Relevant for Protein and Algal Cell Resistance, Langmuir. 25 (2009) 10077–10082. https://doi.org/10.1021/la901038g.
[38] X. Wang, Y. Zhu, T.R. Olsen, N. Sun, W. Zhang, R. Pei, Q. Lin, A graphene aptasensor for biomarker detection in human serum, Electrochimica Acta. 290 (2018) 356–363. https://doi.org/10.1016/j.electacta.2018.08.062.
[39] N. Cennamo, L. Pasquardini, F. Arcadio, L.E. Vanzetti, A.M. Bossi, L. Zeni, D-shaped plastic optical fibre aptasensor for fast thrombin detection in nanomolar range, Sci. Rep. 9 (2019) 1–9. https://doi.org/10.1038/s41598-019-55248-x.
[40] N. Hui, X. Sun, S. Niu, X. Luo, PEGylated Polyaniline Nanofibers: Antifouling and Conducting Biomaterial for Electrochemical DNA Sensing, ACS Appl. Mater. Interfaces. 9 (2017) 2914–2923. https://doi.org/10.1021/acsami.6b11682.
[41] K. Kaneko, M. Hara, T. Nishino, T. Maruyama, One-step biotinylation of cellulose paper by polymer-coating to prepare a paper-based analytical device, Anal. Chem. (2019). https://doi.org/10.1021/acs.analchem.9b04373.
[42] G. Wang, Q. Xu, L. Liu, X. Su, J. Lin, G. Xu, X. Luo, Mixed Self-Assembly of Polyethylene Glycol and Aptamer on Polydopamine Surface for Highly Sensitive and Low-Fouling Detection of Adenosine Triphosphate in Complex Media, ACS Appl. Mater. Interfaces. 9 (2017) 31153–31160. https://doi.org/10.1021/acsami.7b09529.
[43] T. Zhang, Z. Xu, H. Xu, Y. Gu, Y. Xing, X. Yan, H. Liu, N. Lu, Y. Song, S. Zhang, Z. Zhang, M. Yang, Catechol and zwitterion-bifunctionalized poly(ethylene glycol) based

ultrasensitive antifouling electrochemical aptasensor for the quantification of adenosine triphosphate in biological media, Sens. Actuators B Chem. 288 (2019) 469–475. https://doi.org/10.1016/j.snb.2019.03.027.
[44] F. Schröper, D. Brüggemann, Y. Mourzina, B. Wolfrum, A. Offenhäusser, D. Mayer, Analyzing the electroactive surface of gold nanopillars by electrochemical methods for electrode miniaturization, Electrochimica Acta. 53 (2008) 6265–6272. https://doi.org/10.1016/j.electacta.2008.03.068.
[45] G. Sauerbrey, Verwendung von Schwingquarzen zur Wägung dünner Schichten und zur Mikrowägung, Z. Für Phys. 155 (1959) 206–222. https://doi.org/10.1007/BF01337937.
[46] X. Liu, C. Cheng, J. Wu, S. Eda, Y. Guo, A low cost and palm-size analyzer for rapid and sensitive protein detection by AC electrokinetics capacitive sensing, Biosens. Bioelectron. 90 (2017) 83–90. https://doi.org/10.1016/j.bios.2016.10.098.
[47] X. Liu, K. Yang, A. Wadhwa, S. Eda, S. Li, J. Wu, Development of an AC electrokinetics-based immunoassay system for on-site serodiagnosis of infectious diseases, Sens. Actuators Phys. 171 (2011) 406–413. https://doi.org/10.1016/j.sna.2011.08.007.
[48] A.A. Moya, Identification of characteristic time constants in the initial dynamic response of electric double layer capacitors from high-frequency electrochemical impedance, J. Power Sources. 397 (2018) 124–133. https://doi.org/10.1016/j.jpowsour.2018.07.015.
[49] P. Auroy, L. Auvray, Influence of a Polymer Solution on a Polymer Interface, Macromolecules. 29 (1996) 337–342. https://doi.org/10.1021/ma946421g.
[50] H.B. Lu, C.T. Campbell, D.G. Castner, Attachment of Functionalized Poly(ethylene glycol) Films to Gold Surfaces, Langmuir. 16 (2000) 1711–1718. https://doi.org/10.1021/la990221m.
[51] Q. Chen, W. Tang, D. Wang, X. Wu, N. Li, F. Liu, Amplified QCM-D biosensor for protein based on aptamer-functionalized gold nanoparticles, Biosens. Bioelectron. 26 (2010) 575–579. https://doi.org/10.1016/j.bios.2010.07.034.
[52] J. Piehler, A. Brecht, R. Valiokas, B. Liedberg, G. Gauglitz, A high-density poly(ethylene glycol) polymer brush for immobilization on glass-type surfaces, Biosens. Bioelectron. 15 (2000) 473–481. https://doi.org/10.1016/S0956-5663(00)00104-4.
[53] V.L. Koenig, W.L. Carrier, R.O. Rahn, Viscosity studies on dna and the observation of double-stranded and single-stranded breaks in a 40% dmso-phosphate buffer system, Int. J. Biochem. 5 (1974) 601–611. https://doi.org/10.1016/0020-711X(74)90022-6.
[54] Y. Lin, X. Shen, J. Wang, L. Bao, Z. Zhang, D. Pang, Measuring radial Young's modulus of DNA by tapping mode AFM, Chin. Sci. Bull. 52 (2007) 3189–3192. https://doi.org/10.1007/s11434-007-0475-7.
[55] T. Murugesan, M. Perumalsamy, Densities and Viscosities of Polyethylene Glycol 2000 + Salt + Water Systems from (298.15 to 318.15) K, J. Chem. Eng. Data. 50 (2005) 1290–1293. https://doi.org/10.1021/je050035k.
[56] W.J. Price, S.A. Leigh, S.M. Hsu, T.E. Patten, G. Liu, Measuring the Size Dependence of Young's Modulus Using Force Modulation Atomic Force Microscopy, J. Phys. Chem. A. 110 (2006) 1382–1388. https://doi.org/10.1021/jp0544540.
[57] A.B. Steel, R.L. Levicky, T.M. Herne, M.J. Tarlov, Immobilization of Nucleic Acids at Solid Surfaces: Effect of Oligonucleotide Length on Layer Assembly, Biophys. J. 79 (2000) 975–981. https://doi.org/10.1016/S0006-3495(00)76351-X.
[58] H. Wackerbarth, M. Grubb, J. Zhang, A.G. Hansen, J. Ulstrup, Dynamics of Ordered-Domain Formation of DNA fragments on Au(111) with Molecular Resolution, Angew. Chem. Int. Ed. 43 (2004) 198–203. https://doi.org/10.1002/anie.200352146.
[59] J. Zhang, S. Song, L. Wang, D. Pan, C. Fan, A gold nanoparticle-based chronocoulometric DNA sensor for amplified detection of DNA, Nat. Protoc. 2 (2007) 2888–2895. https://doi.org/10.1038/nprot.2007.419.

[60] R. Lao, S. Song, H. Wu, L. Wang, Z. Zhang, L. He, C. Fan, Electrochemical Interrogation of DNA Monolayers on Gold Surfaces, Anal. Chem. 77 (2005) 6475–6480. https://doi.org/10.1021/ac050911x.
[61] G.G. Baralia, A.-S. Duwez, B. Nysten, A.M. Jonas, Kinetics of Exchange of Alkanethiol Monolayers Self-Assembled on Polycrystalline Gold, Langmuir. 21 (2005) 6825–6829. https://doi.org/10.1021/la050245v.
[62] T. Kakiuchi, K. Sato, M. Iida, D. Hobara, S. Imabayashi, K. Niki, Phase Separation of Alkanethiol Self-Assembled Monolayers during the Replacement of Adsorbed Thiolates on Au(111) with Thiols in Solution, Langmuir. 16 (2000) 7238–7244. https://doi.org/10.1021/la991590l.
[63] A.R. Lokanathan, S. Zhang, V.R. Regina, M.A. Cole, R. Ogaki, M. Dong, F. Besenbacher, R.L. Meyer, P. Kingshott, Mixed poly (ethylene glycol) and oligo (ethylene glycol) layers on gold as nonfouling surfaces created by backfilling, Biointerphases. 6 (2011) 180–188. https://doi.org/10.1116/1.3647506.
[64] N. Eliaz, Applications of Electrochemistry and Nanotechnology in Biology and Medicine I, Springer Science & Business Media, 2011.
[65] A. Moody, Rapid Diagnostic Tests for Malaria Parasites, Clin. Microbiol. Rev. 15 (2002) 66–78. https://doi.org/10.1128/CMR.15.1.66-78.2002.
[66] S.K. Martin, G.-H. Rajasekariah, G. Awinda, J. Waitumbi, C. Kifude, Unified Parasite Lactate Dehydrogenase and Histidine-Rich Protein ELISA for Quantification of Plasmodium falciparum, Am. J. Trop. Med. Hyg. 80 (2009) 516–522.
[67] P. Jain, S. Das, B. Chakma, P. Goswami, Aptamer-graphene oxide for highly sensitive dual electrochemical detection of Plasmodium lactate dehydrogenase, Anal. Biochem. 514 (2016) 32–37. https://doi.org/10.1016/j.ab.2016.09.013.
[68] S. Lee, D.H. Manjunatha, W. Jeon, C. Ban, Cationic Surfactant-Based Colorimetric Detection of Plasmodium Lactate Dehydrogenase, a Biomarker for Malaria, Using the Specific DNA Aptamer, PLOS ONE. 9 (2014) e100847. https://doi.org/10.1371/journal.pone.0100847.
[69] G. Hartwich, M. Schneider, A Tunable and Versatile Anchoring System for Gold-Surfaces, Proceedings. 1 (2017) 742. https://doi.org/10.3390/proceedings1080742.

Graphical abstract

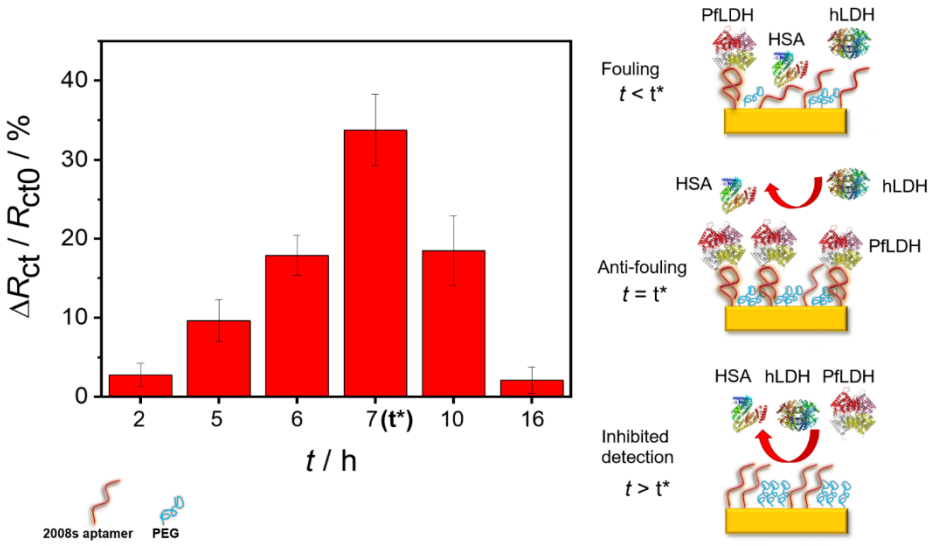

Highlights

- PEG blocking enhances malaria biomarker PfLDH detection in human serum.
- Morphological composition of aptamer/PEG monolayer depends on PEG incubation time.
- Long PEG incubation times leads to phase separation of aptamer and PEG molecules.
- PfLDH detection in full human serum with LOD of 1.49 pM.
- Type of blocking molecule has no influence of sensor sensitivity.

Figure captions

Scheme 1. Schematic illustration of varying aptamer/PEG morphologies on a gold surface at different PEG incubation times for optimized PfLDH detection in human serum.

Fig. 1. EIS Nyquist plots of Au electrodes demonstrating the non-specific adsorption on a receptor-free surface covered with a) MCH (red spheres) and b) PEG (red spheres) tested with 50 nM PfLDH (black spheres) in human serum. The inset shows the electrical equivalent Randles circuit at the limit of high-frequency used to fit with the experimental data. The components of the electrical equivalent circuit are: solution resistance, R_s; double layer capacitance represented by a constant phase element, CPE; and charge transfer resistance, R_{ct}.

Fig. 2. a) Complete QCM-D plot for aptamer and PEG immobilization and PfLDH detection. Frequency (Δf) and dissipation (ΔD) change after b) aptamer immobilization, c) PEG blocking, and d) 10 and 50 nM PfLDH detection, respectively.

Fig. 3. XPS analysis of a bare gold chip (blue line), gold chip modified with aptamer (red line), and aptamer/PEG modified gold chip (black line). Gold (Au 4f) and traces of carbon (C 1s) photoelectron peaks at 84 and 285 eV, respectively, for a bare gold electrode. After immobilization of aptamer/ and PEG, the appearance of the oxygen (O 1s, 533 eV), nitrogen (N 1s, 400 eV), phosphorous (P 2p, 134 eV) and sulfur (S 2p, 164 eV) peaks were evident.

Fig. 4. Tapping mode AFM image and line cross section for a bare single crystal gold (111) surface (a, b), after aptamer immobilization (c, d), and additional PEG binding for 2 h (e, f), 7 h PEG (g, h); and 16 h PEG (i, j). The bottom schematics depict the change of

the composition of the mixed aptamer/PEG receptor layer for the corresponding preparation conditions. The color scale of a) goes from -1.2 nm to 1.2 nm; the color scales from c) – i) go from -2 to 2 nm.

Fig. 5. Optimization time of PEG blocking with 10 nM PfLDH detection. The experiments have been repeated three times with different sensor devices.

Fig. 6. Calibration curves of PfLDH detection in human serum by using a) MCH or b) PEG blocking molecules in *in situ* measurement, and c) PEG blocking molecule in *ex situ* measurement. The experiments have been repeated three times with different sensor devices.

Fig. 7. Selectivity of PfLDH detection vs. analogous proteins in human serum at 50 nM concentration for all proteins. The experiments have been repeated three times with different sensor devices.

Scheme 1 (two column)

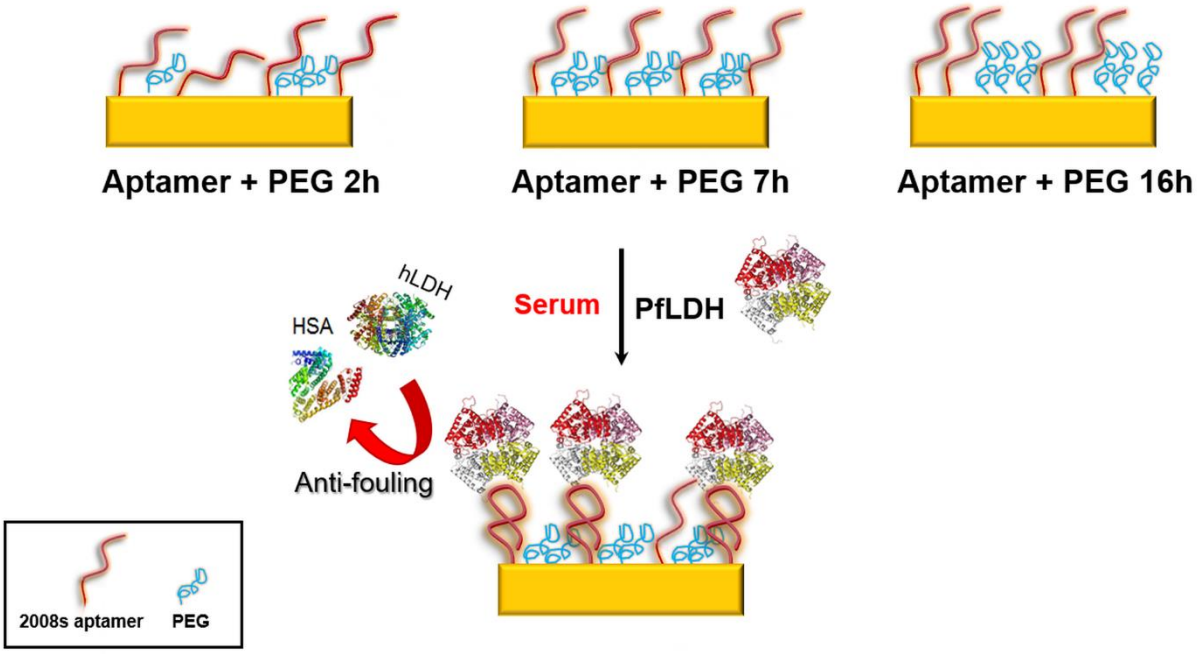

Fig. 1 (two column)

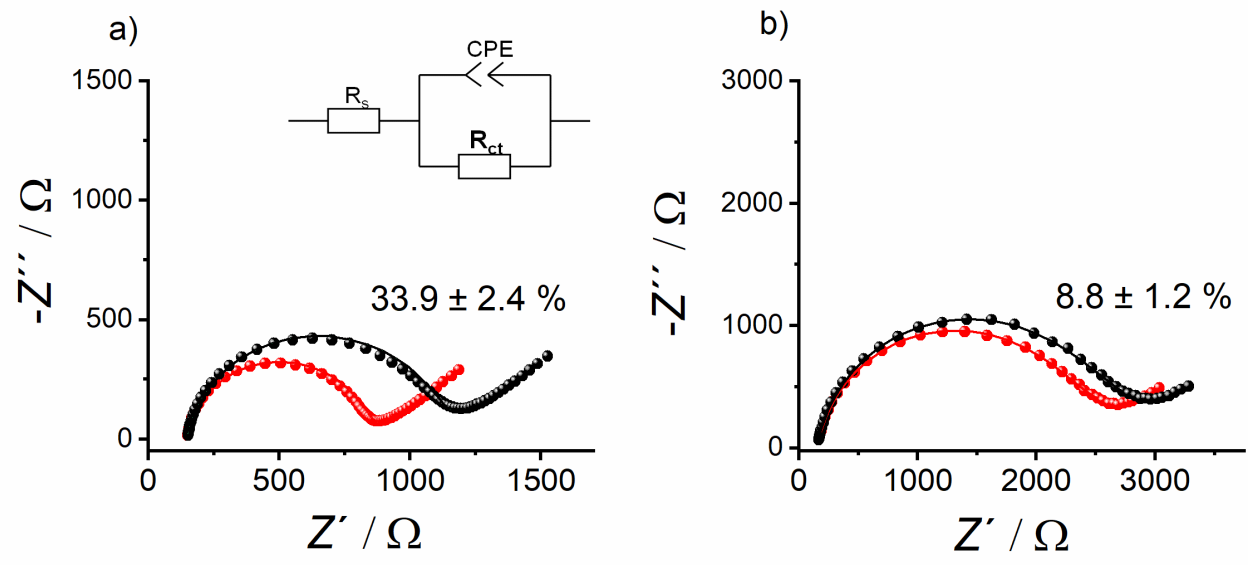

Fig. 2 (two column)

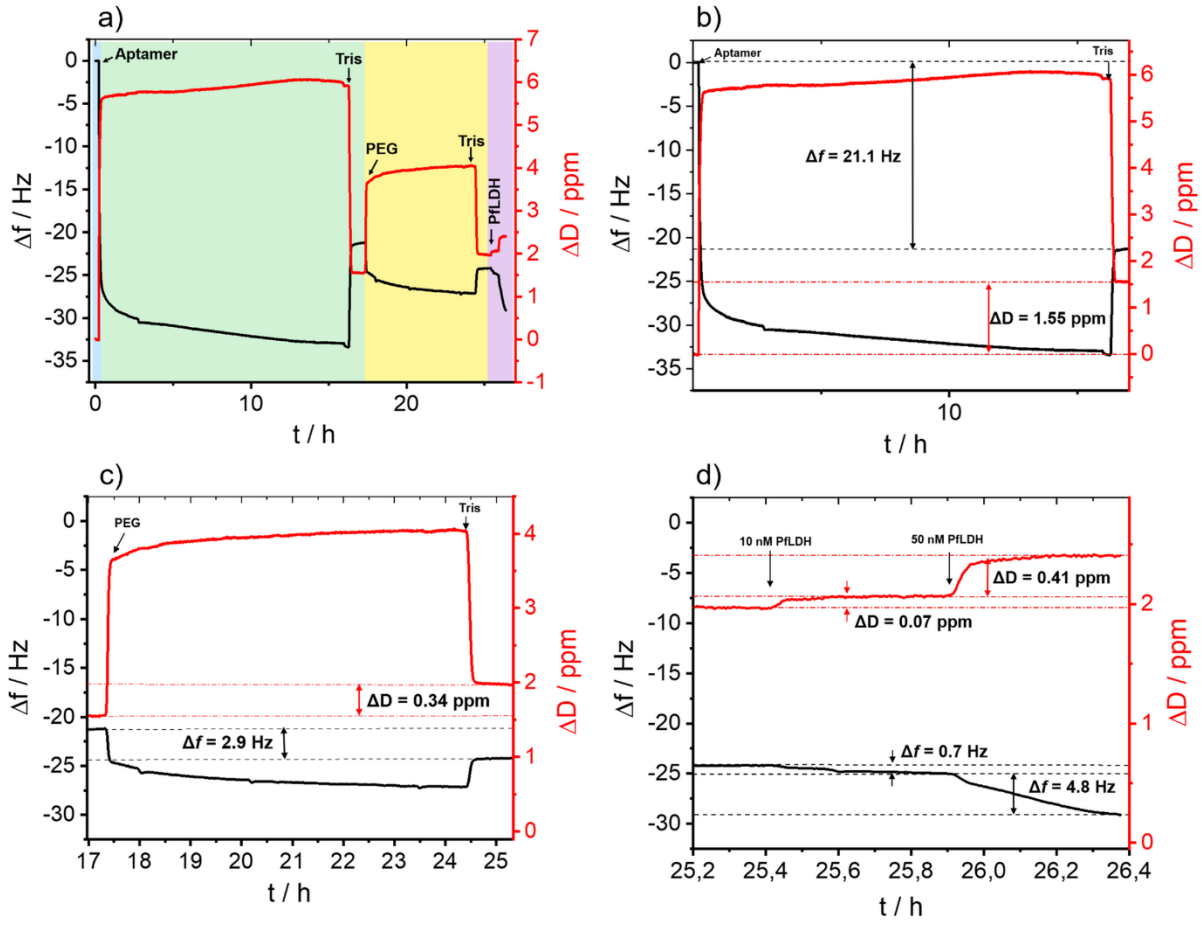

Fig. 3 (1.5 column)

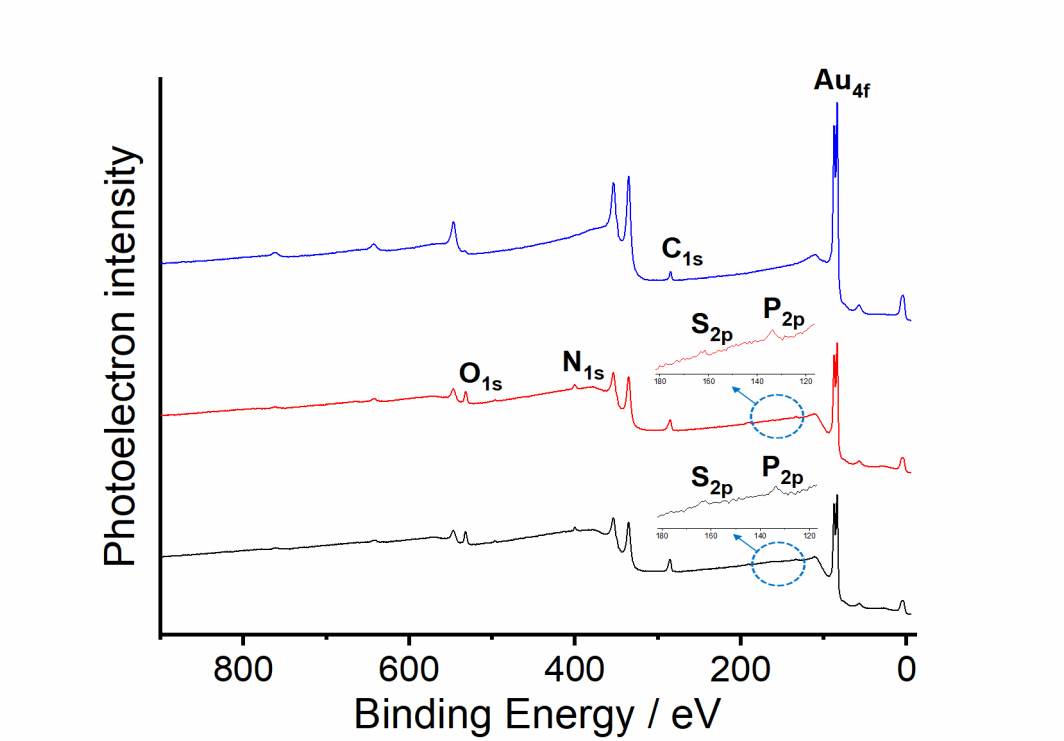

Fig. 4 (two column)

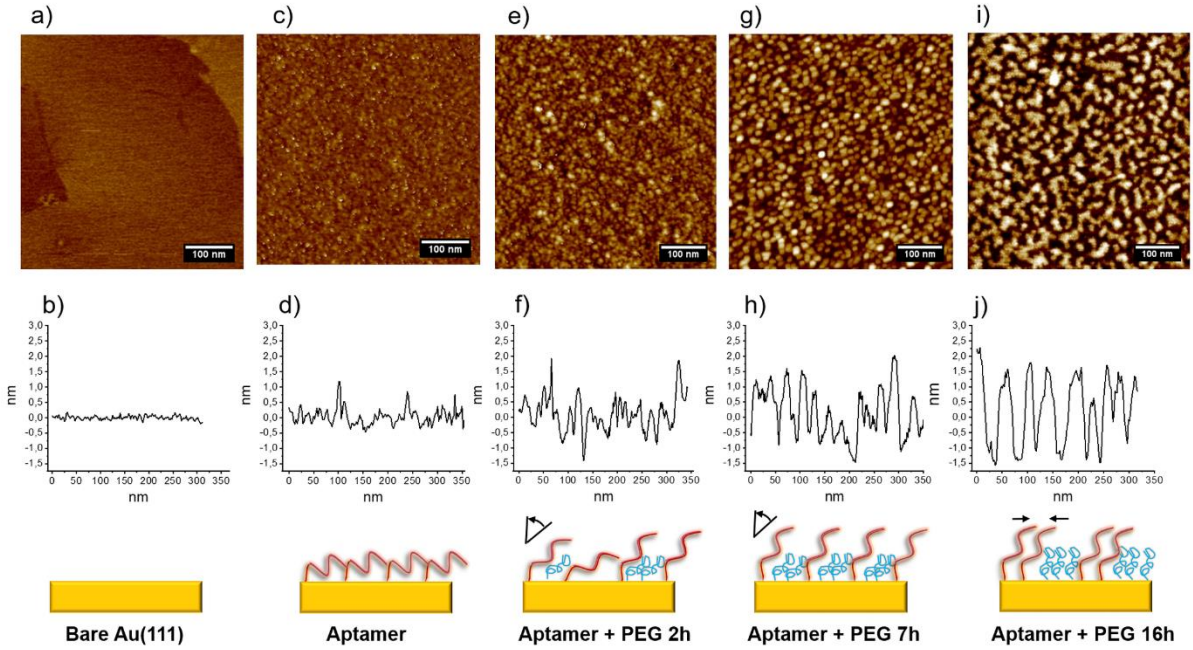

Fig. 5 (single column)

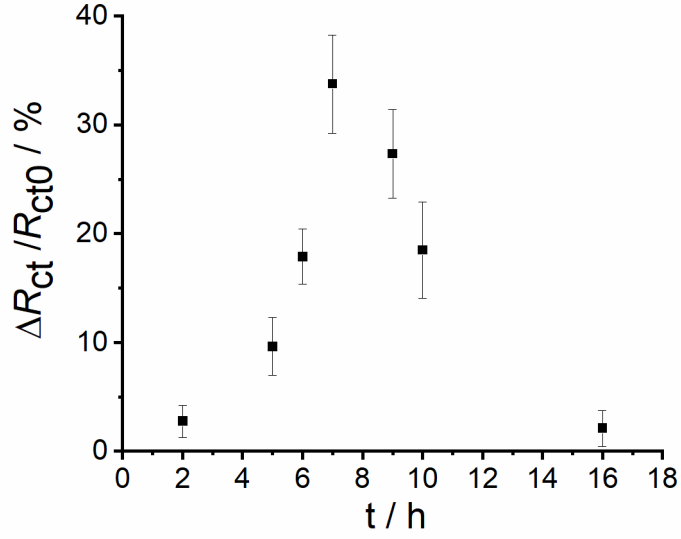

Fig. 6 (two column)

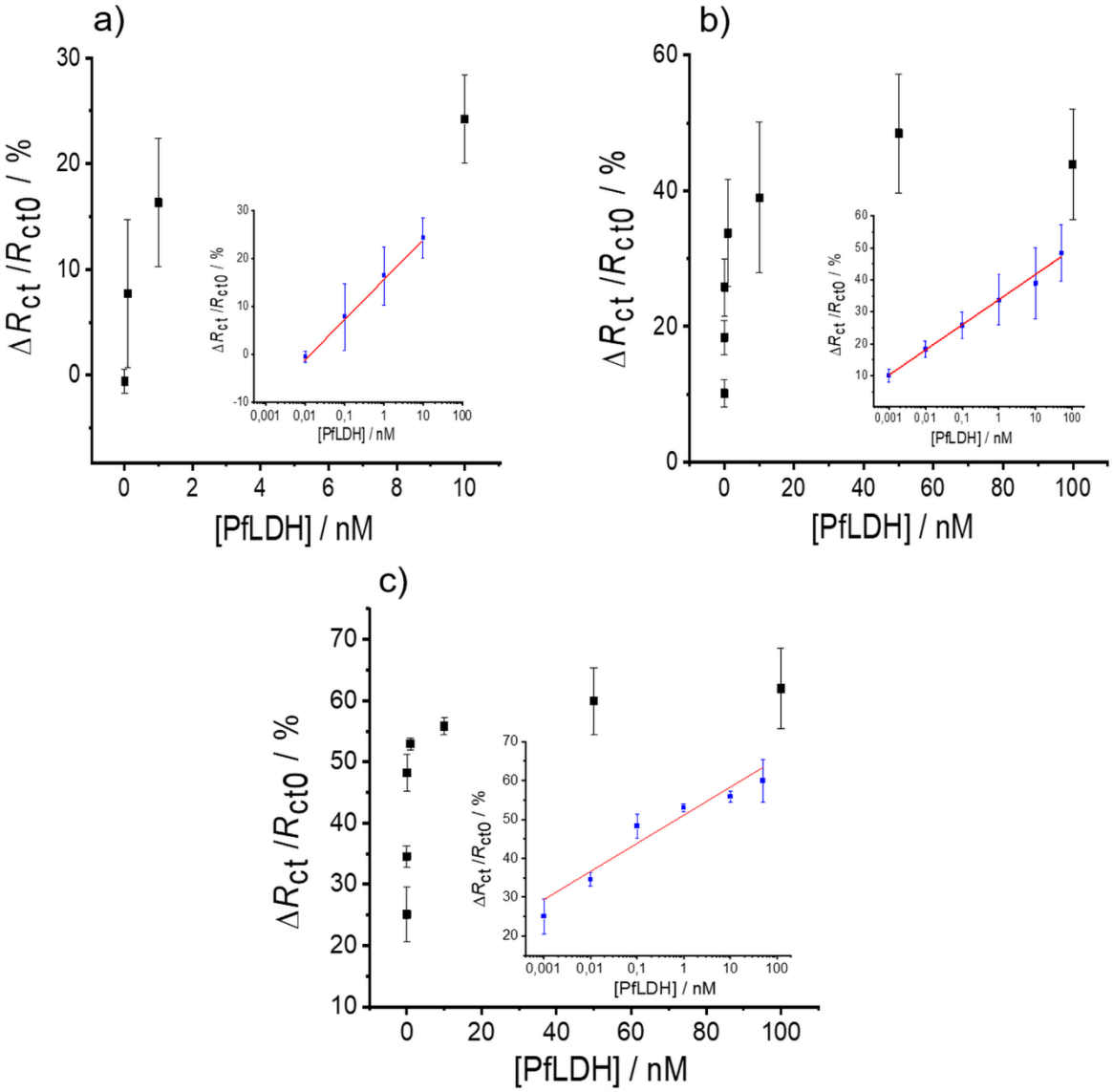

Fig. 7 (single column)